

## Article

# Comprehensive Growth Index (CGI): A Comprehensive Indicator from UAV-Observed Data for Winter Wheat Growth Status Monitoring

Yuanyuan Tang <sup>1,2</sup>, Yuzhuang Zhou <sup>1,2</sup>, Minghan Cheng <sup>1,2</sup> and Chengming Sun <sup>1,2,\*</sup> 

<sup>1</sup> Jiangsu Key Laboratory of Crop Genetics and Physiology/Jiangsu Key Laboratory of Crop Cultivation and Physiology, Agricultural College, Yangzhou University, Yangzhou 225009, China; 211702111@stu.yzu.edu.cn (Y.T.); 213210714@stu.yzu.edu.cn (Y.Z.); 008170@yzu.edu.cn (M.C.)

<sup>2</sup> Jiangsu Co-Innovation Center for Modern Production Technology of Grain Crops, Yangzhou University, Yangzhou 225009, China

\* Correspondence: cmsun@yzu.edu.cn

**Abstract:** Crop growth monitoring plays an important role in estimating the scale of food production and providing a decision-making basis for agricultural policies. Moreover, it can allow understanding of the growth status of crops, seedling conditions, and changes in a timely manner, overcoming the disadvantages of traditional monitoring methods such as low efficiency and inaccuracy. In order to realize rapid and non-destructive monitoring of winter wheat growth status, this study introduced an equal weight method and coefficient of variation method to construct new comprehensive growth indicators based on drone images and measured data obtained from field experiments. The accuracy of the indicators in evaluating the growth of winter wheat can be judged by the construction, and the effects of different machine learning methods on the construction of indicators can be compared. Correlation analysis and variable screening were carried out on the constructed comprehensive growth indicators and the characteristic parameters extracted by the drone, and the comprehensive growth index estimation model was constructed using the selected parameter combination. Among them, when estimating the comprehensive growth index (CGI<sub>avg</sub>), the optimal model at the jointing stage is the support vector regression (SVR) model: R<sub>2</sub> is 0.77, RMSE is 0.095; at the booting stage, the optimal model is the Gaussian process regression (GPR) model: R<sub>2</sub> is 0.71, RMSE is 0.098; at the flowering stage, the optimal model is the SVR model: R<sub>2</sub> is 0.78, RMSE is 0.087. When estimating the comprehensive growth index based on the coefficient of variation method (CGI<sub>cv</sub>), the optimal model at the jointing stage is the multi-scale retinex (MSR) model: R<sub>2</sub> is 0.73, RMSE is 0.084; at the booting stage, the optimal model is the GPR model: R<sub>2</sub> is 0.74, RMSE is 0.092; at the flowering stage, the optimal model is the SVR model, R<sub>2</sub> is 0.78: RMSE is 0.085. The conclusion shows that the method of constructing the comprehensive growth index is superior to the function of a single parameter to some extent, providing a new way for wheat growth monitoring and process management.

**Keywords:** winter wheat; UAV images; machine learning; equal weight method; coefficient of variation method



**Citation:** Tang, Y.; Zhou, Y.; Cheng, M.; Sun, C. Comprehensive Growth Index (CGI): A Comprehensive Indicator from UAV-Observed Data for Winter Wheat Growth Status Monitoring. *Agronomy* **2023**, *13*, 2883. <https://doi.org/10.3390/agronomy13122883>

Academic Editors: Mavromatis Theodoros, Thomas Alexandridis and Vassilis Aschonitis

Received: 16 October 2023

Revised: 12 November 2023

Accepted: 17 November 2023

Published: 24 November 2023



**Copyright:** © 2023 by the authors. Licensee MDPI, Basel, Switzerland. This article is an open access article distributed under the terms and conditions of the Creative Commons Attribution (CC BY) license (<https://creativecommons.org/licenses/by/4.0/>).

## 1. Introduction

In recent years, with the advancement of science and technology and the rapid development of modern agriculture, the planting and management of crops have gradually become more scientific and precise [1]. As one of the main food crops in China, the monitoring and evaluation of the growth status of wheat is crucial to the scientific decision making and management of agricultural production [2].

Wheat growth monitoring based on comprehensive growth indicators is one of the feasible methods for wheat growth monitoring at present. It comprehensively and accurately evaluates and predicts the growth status of wheat through comprehensive monitoring of

various indicators in the wheat growth process by combining appropriate models and algorithms. This method can not only help managers understand the status of wheat growth in a timely manner, take measures to control pests and diseases, and ensure wheat yield and quality, but also promote the continuous upgrading and progress of wheat planting technology. However, there are also challenges and difficulties in wheat growth monitoring based on comprehensive growth indicators. First, wheat growth is affected by many factors, and all indicators cannot be comprehensively analyzed. Second, the monitoring and evaluation of wheat growth status needs to establish appropriate mathematical models and algorithms and reasonably weight and calculate the monitoring indicators so as to obtain accurate evaluation results. Finally, wheat growth monitoring based on comprehensive growth indicators requires the support of a large amount of data, and the cost and difficulty of data collection and processing are also some of the current difficulties.

Feng et al. [3] studied the use of drone remote sensing data to monitor crop growth; combined single parameters such as plant nitrogen content, aboveground biomass, plant water content, and leaf chlorophyll content to obtain a comprehensive growth index (CGI); and obtained a CGI through UAV-observed hyperspectral parameters. The estimated CGI was better than the RGB color index. Zhao Xin et al. [4] constructed a comprehensive crop growth index, and the study showed that the correlation between the comprehensive index and crop yield was better than that of a single index and had a better growth-monitoring effect. Zhou et al. [5] extracted the Landsat normalized difference vegetation index (NDVI) and temperature–vegetation dryness index (VTCDI) time series of winter wheat at the heading stage and calculated the corresponding weights to construct a comprehensive crop growth monitoring index. The results show that the monitoring accuracy of the constructed comprehensive index was better than that of a single index. Zhai et al. [6] used information entropy to calculate the weight of a single index and constructed a new comprehensive index to analyze the growth of winter wheat. The results showed that the inversion accuracy of the comprehensive growth index (CGI) of winter wheat based on the spectral index was the highest. Pei Haojie et al. [7] proposed the construction of a comprehensive growth index (CGI) using equal weights of indicators such as the leaf area index, leaf chlorophyll content, plant nitrogen content, and plant water content. The results showed that the comprehensive growth index (CGI) retrieved from drone hyperspectral images had high accuracy, which can provide a reference for monitoring the growth status of wheat. Wang et al. used principal component analysis (PCA) to construct a comprehensive growth index (CGI) and partial least squares regression (PLSR) to construct a hyperspectral prediction model of agronomic parameters. The accuracy and robustness of their CGI model were verified, showing that the combination of remote sensing technology and multivariate statistical analysis has great potential in the crop field [8].

In this study, a comprehensive growth index (CGI) that aims to comprehensively characterize the growth status of winter wheat was constructed by combining multiple agronomic parameters. Through this study, we can realize the monitoring of wheat growth and provide a theoretical and practical basis for the promotion and application of UAV image data.

## 2. Materials and Methods

### 2.1. Study Area and Experimental Design

During the 2020–2021 wheat planting season, the test site was located in the experimental field of Fengling Reservoir, Dayi Town, Yizheng City, China (32°30' N, 119°13' E). The three tested varieties involved in the experiment were all spring wheat, namely Yangmai 23 (P1), Zhengmai 9 (P2), and Ningmai 13 (P3). The previous stubble of the field was planted with rice, and the soil was clay loam. The organic matter content of the tillage layer was 23.64 g/kg, the available nitrogen content was 55.23 mg/kg, the available phosphorus content was 23.43 mg/kg, and the available potassium content was 82.37 mg/kg. All fertilizers were applied before sowing, including resin-coated controlled-release nitrogen fertilizers

with a controlled-release period of 180 days and a nitrogen content of 44%, superphosphate with a  $P_2O_5$  content of 12%, and KCl with a  $K_2O$  content of 60%.

The random factors of the experiment were seeding density and nitrogen fertilizer level. As shown in Figure 1, the varieties (P) of wheat were Yangmai 23, Zhengmai 9, and Ningmai 13; the density treatments (M) M1 and M2 were 225 plants/ $m^2$  and 300 plants/ $m^2$ . The nitrogen fertilizer layers (N) were 225 kg/ $hm^2$ , 202.5 kg/ $hm^2$ , 180 kg/ $hm^2$ , and 157.5 kg/ $hm^2$ .

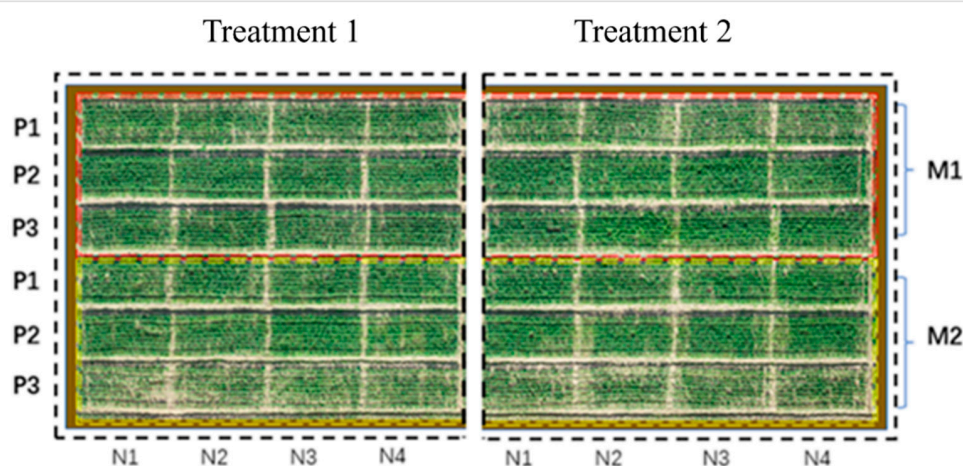


**Figure 1.** Orthophoto image of the test field taken with a drone.

## 2.2. Data Acquisition and Processing

### 2.2.1. Acquisition and Processing of Drone Image Data

#### Drone RGB Image Acquisition

The drone equipment used in this test is the DJI PHANTOM 4 RTK drone manufactured by DJ Company. The Genie 4RTK drone is a high-performance aerial survey drone. The aircraft uses dual-redundancy MU and compass to improve safety performance, and the positioning system adopts dual backup systems. Advanced flight control and a high-precision positioning system ensure the accuracy of mission flight and provide strong technical support for experimental shooting. The sensors carried by the drone have the function of obtaining high-definition image data, and the lenses of each camera can ensure the accuracy of imaging.

In this study, images were taken at the jointing stage, booting stage, and flowering stage of wheat. The flight height of the drone was set to 25 m in the experiment, and the route was drawn in the experimental area to realize automatic flight and image acquisition at equal time intervals. The drone was used from 10:30 am to 11:30 am on the day of sampling, and sunny weather conditions were selected to avoid the intervention of strong winds.

#### Acquisition of Drone Hyperspectral Image Data

In order to obtain hyperspectral image data of wheat, the Gaiasky-Mini2 hyperspectral imaging system produced by Shuangli Spectrum was combined with the Jingwei M600 PRO produced by DJ Company to obtain hyperspectral data images of the experimental field. The Gaiasky-Mini2 airborne hyperspectral imaging system has an extremely low system cost and test cost and adopts a hover shooting method. This M600 PRO drone continues the high load and excellent performance of the previous M600, improving the efficiency of image acquisition.

In the experiment, the flight altitude of the M600 PRO was set to 100 m, and the route planning was carried out in the test area. The lens was checked before the flight to determine whether the exposure time had been calibrated. A gray cloth needed to be laid in the test area as a reference for later image calibration. Image acquisition was carried out at the jointing

stage, booting stage, and flowering stage of wheat. The UAV campaigns occurred during 10:30–11:30 a.m. The weather should be sunny and not affected by strong winds.

### 2.2.2. Determination of Wheat Agronomic Parameters Aboveground Biomass Determination

During sampling, 25 wheat plants with relatively uniform growth were randomly selected for each treatment. The roots were rinsed with water, and the stems, leaves, and ears were decomposed. After the fresh weight was measured, it was bagged and put into an oven to adjust the temperature to 105 °C. The wheat was baked for 30 min, then the temperature was reduced to 80 °C and the sample continued to dry until it was a constant weight. Then, the sample was weighed and the obtained dry weight was converted to the dry weight of the ground per unit area (kg/hm<sup>2</sup>).

### Soil and Plant Analyzer Development (SPAD) Value Determination

Ten wheat plants with uniform growth were randomly selected in the field. The inverted 2 leaves of the wheat plants were measured at the jointing stage, and the flag leaves of the wheat plants were measured at the booting stage and flowering stage. The mean value was obtained by measuring the three positions of the leaf tip, leaf middle, and leaf root with a portable SPAD-502 chlorophyll meter.

### Determination of Nitrogen Content in Leaves

The wheat plants sampled in the field were treated and dried, and then the leaf samples were ground and crushed, and 0.25 g was weighed according to the experimental treatment. The nitrogen content of the wheat leaves was determined using the H<sub>2</sub>SO<sub>4</sub>–H<sub>2</sub>O<sub>2</sub> digestion method and repeated three times.

## 2.3. Methodology

### 2.3.1. Feature Parameter Extraction

#### Extraction of Color Index

The principle of extracting the color index from drone RGB images is based on the different ability of light of different wavelengths to reflect on the surface of the object. By measuring the intensity and wavelength of the reflected light, the color of the object can be inferred. Therefore, separating the RGB image into different color channels can extract the color information of the target area. At the same time, calculating different color indices can extract different characteristics of the target area according to different needs. In this study, 10 common color indices were selected for analysis. The calculation methods of each color index are shown in Table 1.

$$r = \frac{R}{R + G + B}$$

$$g = \frac{G}{R + G + B}$$

$$b = \frac{B}{R + G + B}$$

#### Extraction of Vegetation Index

The principle of the vegetation index is based on the reflectivity characteristics of vegetation in different bands. Through the hyperspectral image data captured using the drone, all bands in the image are extracted, and the required vegetation index is calculated through a specific formula. In this study, 12 vegetation indices were selected, and Table 2 shows the selected vegetation indices and their calculation methods.

**Table 1.** Selected color indices and their calculation methods.

Parameters	Equation	References
Visible atmospherically resistant index (VARI)	$(g - r)/(g + r - b)$	[9]
Excess green vegetation index (ExG)	$2 \times g - r - b$	[10]
Modified GRVI (MGRVI)	$(g^2 - r^2)/(g^2 + r^2)$	[10]
Neighborhood deprivation index (NDI)	$(r - g)/(r + g + 0.01)$	[10]
Excess green minus excess red index (ExGR)	$3 \times g - 2.4 \times r - b$	[10]
Red–green–blue vegetation index (RGBVI)	$(g^2 - b \times r)/(g^2 + b \times r)$	[11]
Red–green ratio index (RGRI)	$R/G$	[11]
Normalized green–blue difference index (NGBDI)	$(G - B)/(G + B)$	[11]
Normalized pigment chlorophyll index (NPCI)	$(R - B)/(R + B)$	[12]
Vegetative index (VEG)	$G/(R^{0.667} \times B^{0.33})$	[12]

Note: R, G, and B refer to the average DN values of red, green, and blue bands, respectively. r, g, and b refer to the normalized values of R, G, and B, respectively. The calculation method is as follows.

**Table 2.** Selected vegetation indices and their calculation methods.

Parameters	Equation	References
Normalized difference vegetation index (NDVI)	$(R800 - R680)/(R800 + R680)$	[13]
Radar vegetation index (RVI)	$R800/R680$	[13]
Difference vegetation index (DVI)	$R800 - R680$	[13]
Optimized soil-adjusted vegetation index (OSAVI)	$(1 + 0.16) \times (R800 - R670)/(R800 + R670 + 0.16)$	[14]
Renormalized difference vegetation index (RDVI)	$(R800 - R680)/(R800 + R680)$	[14]
Vogelmann index (VOGI)	$R740/R720$	[14]
Enhanced vegetation index (EVI)	$2.5 \times (R860 - R645)/(1 + R860 + 6 \times R645 - 7.5 \times R470)$	[14]
Green normalized difference vegetation index (GNDVI)	$(R750 - R550)/(R750 + R550)$	[15]
Modified simple ratio (MSR)	$(R750/R705 - 1)/((R750/R705) + 1)$	[15]
Modified soil adjusted vegetation index (MSAVI)	$[2 \times R750 + 1 - ((2 \times R750 + 1)^2 - 8 \times (R750 - R705))^{0.5}]/2$	[15]
Plant senescence/reflectance index (PSRI)	$(R680 - R500)/R750$	[16]
Transformed chlorophyll absorption and reflectance index (TCARI)	$3 \times [(R700 - R670) - 0.2 \times (R700 - R550) \times (R700/R670)]$	[16]

Note: Rx refers to the reflectance of the x nm band.

### 2.3.2. Feature-Screening Methods

#### CARS Algorithm

Competitive adaptive re-weighted sampling (CARS) is a combination of Monte Carlo sampling and the characteristic variable selection method of the regression coefficient of the PLS model. The point with the larger absolute value weight of the regression coefficient in the PLS model is selected as a new subset, the outlier is deleted, and the PLS model is constructed through the established subset. With an increase in the number of runs, the wavelength in the subset with the smallest root mean square error (RMSECV) of the PLS model is selected as the characteristic wavelength [17].

#### SPA Algorithm

The successive projections algorithm (SPA) is a forward iterative search method that starts with a wavelength and adds a new variable at each iteration until the number of selected variables reaches the set value N. The function of this algorithm is to select the wavelength with the least redundancy in spectral information to solve its collinearity problem [18].

### 2.3.3. Modeling Methods

#### Multiple Regression

Multivariate stepwise regression (MSR) is a commonly used multivariate linear regression analysis method that can help us determine the best combination of variables, build a

multivariate regression model, and predict the value of the dependent variable. Multiple stepwise regression modeling is used to select the most relevant independent variable to explain the change in the dependent variable. This method is based on the idea of stepwise regression, which builds the best multiple linear regression model by gradually adding and removing independent variables [19].

The principle of multiple stepwise regression modeling is to select variables that can significantly improve the performance of the model in the process of gradually adding and removing independent variables and eliminate variables that do not contribute or contribute little to the performance of the model. Through this method, the model can be simplified, and the predictive power and interpretability of the model can be improved.

#### Support Vector Machine Regression

The support vector regression (SVR) method is a support vector machine (SVM)-based nonparametric regression method suitable for processing datasets with continuous outputs. For a given training dataset, the SVR model attempts to learn a nonlinear function that predicts the value of the dependent variable. The function maps the independent variables into a high-dimensional space and builds a hyperplane in that space such that the distance from the training data point to that hyperplane is minimized. The loss function of support vector machine regression is epsilon-insensitive, that is, when the gap between the training data points and the predicted value of the model is less than a certain threshold epsilon, the loss is 0; otherwise, the loss is the absolute value of the gap. At the same time, the model needs to satisfy the prediction error while maximizing the interval of the hyperplane. When solving the SVR model, it is necessary to find the optimal solution by solving a quadratic programming problem [20].

#### Gaussian Process Regression

The Gaussian process regression (GPR) method is a nonparametric regression method based on Bayesian theory. The goal is to model an unknown function through a Gaussian distribution, using known training data to learn the parameters of the function. Based on the prior distribution and the training dataset, the posterior distribution can be calculated using Bayes' theorem, which is the distribution of predicted value  $y$  for the new input  $x$ . This distribution is a Gaussian distribution whose mean and variance can be calculated from the prior distribution, training data, and covariance functions. In practical applications, appropriate kernel functions and noise standard deviations are selected and hyperparameters are adjusted to obtain a better prediction performance [21].

#### Comprehensive Growth Index (CGI)

The measured biomass, chlorophyll content, and leaf nitrogen content were normalized (Equation (1)) to make them comparable. Using the equal weight method, the weights of biomass, chlorophyll content, and leaf nitrogen content were set to 1/3. Then (Equation (2)) multiplied the normalized biomass, chlorophyll content, and leaf nitrogen content by their corresponding weights and then added them to obtain a comprehensive growth index ( $CGI_{avg}$ ).

$$I_i = \frac{X_i - X_{i \min}}{X_{i \max} - X_{i \min}} \quad (1)$$

$$CGI_{avg} = \sum_{i=1}^n \frac{1}{3} \times I_i \quad (2)$$

where  $i$  represents the category of agronomic parameters,  $I_i$  represents the normalized class  $i$  parameters,  $X_i$  represents the original class  $i$  parameters (including above-ground biomass (AGB), leaf N concentration (LNC), and SPAD),  $X_{i \max}$  represents the maximum value of the class  $i$  agronomic parameters in the same growth period, and  $X_{i \min}$  represents the minimum value of the class  $i$  agronomic parameters in the same growth period.

#### 2.4. Evaluation Indicators of the Model

For model evaluation, this study selects three commonly used evaluation indicators, namely, the determination coefficient  $R^2$ , root mean square error  $RMSE$ , and normalized root mean square error  $NRMSE$ .

$$R^2 = \frac{\sum_{i=1}^n (X_i - \bar{X}_i)^2 \times (X_i - \bar{Y}_i)^2}{\sum_{i=1}^n (X_i - \bar{X}_i)^2 \times \sum_{i=1}^n (Y_i - \bar{Y}_i)^2} \quad (3)$$

$$RMSE = \sqrt{\frac{1}{n} \sum_{i=1}^n ((Y_i - X_i)^2)} \quad (4)$$

$$NRMSE = \frac{RMSE}{X_i} \quad (5)$$

where  $X_i$ ,  $\bar{X}_i$ ,  $Y_i$ , and  $\bar{Y}_i$  are the measured values, measured mean values, predicted values, and predicted value mean values, respectively;  $n$  is the sample size.

### 3. Results

#### 3.1. Construction of Comprehensive Growth Indicators Based on Different Methods

##### 3.1.1. Construction of Comprehensive Growth Index Based on Equal Weight Method

The healthy growth of crops and high-yield and high-quality production require quantitative monitoring and evaluation. The above-ground biomass, chlorophyll content, and leaf nitrogen content are all important indicators to characterize crop health. However, these indicators alone cannot comprehensively evaluate the growth status of crops. Therefore, this study will use the equal weight method, combining the three indicators of above-ground biomass, chlorophyll content, and leaf nitrogen content, to construct a new comprehensive index to comprehensively evaluate the growth status of crops.

In order to ensure the accuracy and representativeness of the CGI established based on the equal weight method in terms of growth monitoring, it is necessary to further analyze the correlation between the CGI constructed based on the equal weight method and various agronomic parameters. The results are shown in Table 3. The results show that the CGI constructed based on the equal weight method has a very significant correlation level with aboveground biomass, chlorophyll content, and leaf nitrogen content, indicating that the CGIavg constructed based on the equal weight method can characterize wheat growth information.

**Table 3.** Correlation analysis of agronomic parameters and comprehensive index CGIavg in each growth stage.

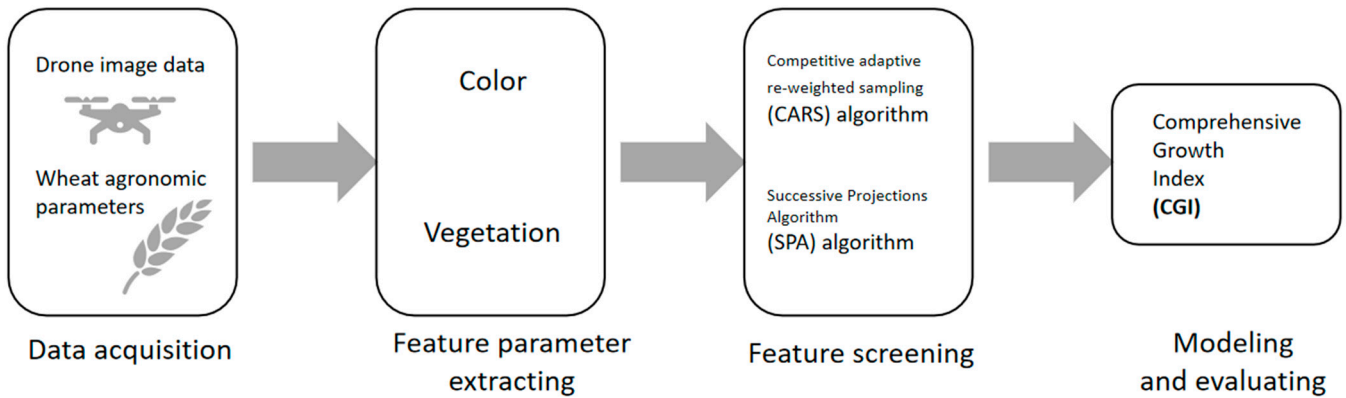
Growth Stage	AGB	SPAD	LNC
Jointing Stage	0.910 **	0.782 **	0.727 **
Booting Stage	0.900 **	0.854 **	0.893 **
Flowering Stage	0.884 **	0.851 **	0.771 **

Note: \*\* indicate significance at 0.01 level, respectively.

Table 3 shows the correlation analysis of CGI with above-ground biomass (AGB), SPAD, and leaf N concentration (LNC). At the jointing stage, the correlation coefficient of CGI with AGB, SPAD, and LNC is 0.91, 0.78, 0.73, respectively. At the booting stage, the correlation coefficient between CGI and AGB, SPAD, and LNC is 0.90, 0.85, and 0.89, respectively. At the flowering stage, the correlation coefficient between CGI and AGB, SPAD, and LNC is 0.88, 0.85, and 0.77, respectively.

In this section, the extracted characteristic parameters were used for correlation analysis and feature screening with CGIavg. In this paper, 22 characteristic parameters were selected as the research objects, and the correlation between them and the comprehensive

growth indicators constructed in the three key growth stages of wheat was analyzed. The results are shown in Figures 2–5. Among them, the characteristic parameters of ExG, MGRVI, NDI, ExGR, RGBVI, RGRI, NGBDI, VEG, NDVI, RVI, DVI, OSAVI, RDVI, EVI, MSAVI, PSRI and other characteristic parameters reached a very significant level in each period. Compared with the aboveground biomass, chlorophyll content, and leaf nitrogen content, the correlation levels of NPCI and TCARI in each period were different.



The flowchart of methods

Figure 2. The flowchart of methods.

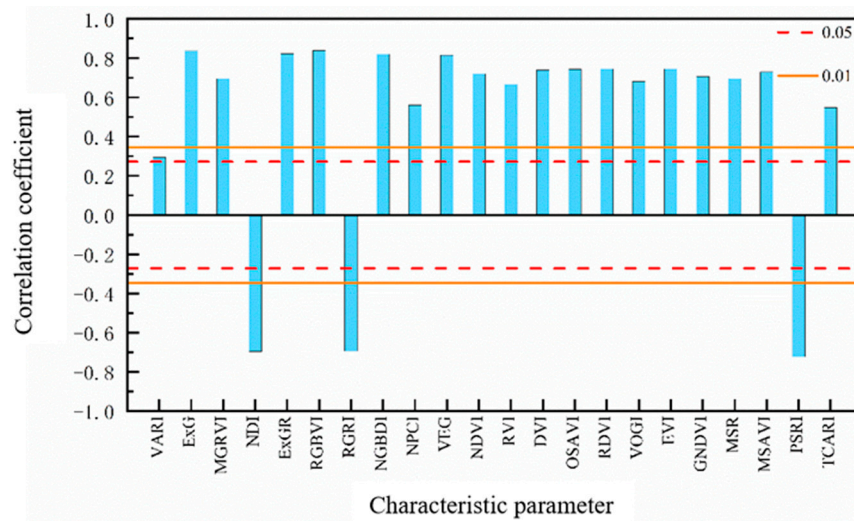
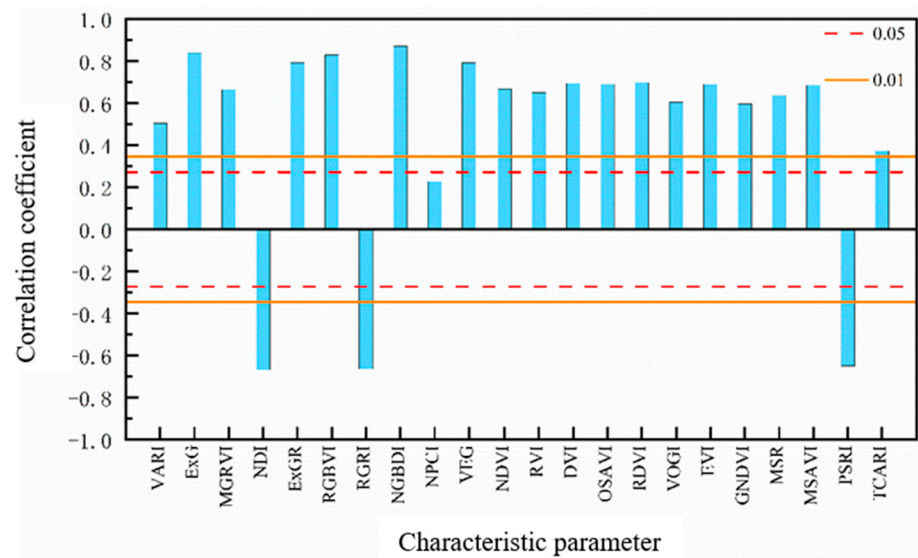
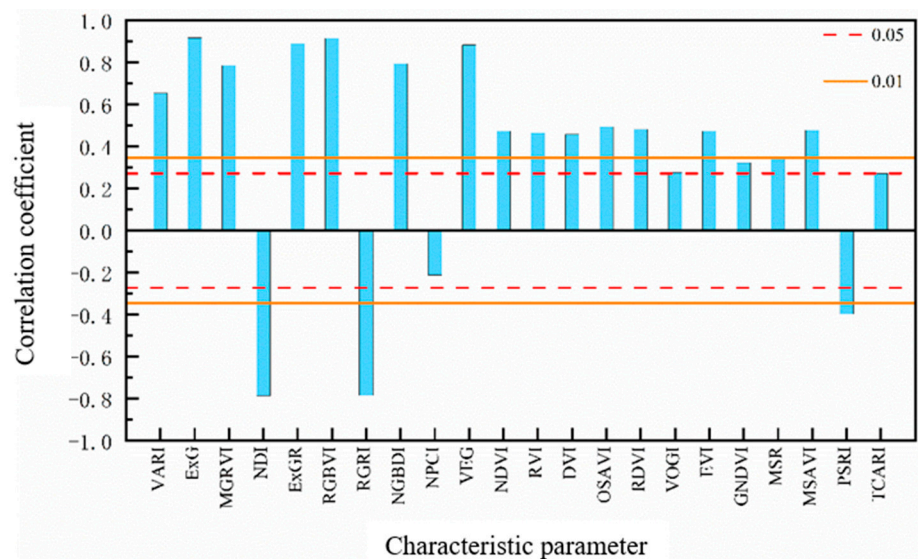


Figure 3. Correlation analysis between the characteristic parameters at the jointing stage and CGIavg. Note: the solid orange line indicates the significance level at  $p > 0.01$ ; the red dotted line indicates the significance level at  $p > 0.05$ .

Figure 6 shows the variable-selection process of the characteristic parameters at the jointing stage, booting stage, and flowering stage through the SPA algorithm. As shown in the figure, the variables selected for the jointing stage were RGBVI and RVI. The screening variables at the booting stage were VARI, NPCI, and EVI. VARI, NGBDI, and VOGI were selected as the variables for the flowering stage.



**Figure 4.** Correlation analysis between characteristic parameters at the booting stage and CGIavg. Note: the solid orange line indicates the significance level at  $p > 0.01$ ; the red dotted line indicates the significance level at  $p > 0.05$ .



**Figure 5.** Correlation analysis between characteristic parameters at the flowering stage and CGIavg. Note: the solid orange line indicates the significance level at  $p > 0.01$ ; the red dotted line indicates the significance level at  $p > 0.05$ .

### 3.1.2. Construction of Comprehensive Growth Index Based on Coefficient of Variation Method

As a commonly used index weight determination method, the coefficient of variation method has a wide range of application values in the construction of comprehensive wheat growth indicators. In this study, first, the measured data of aboveground biomass, leaf nitrogen content, and chlorophyll content of wheat in each period were normalized to avoid errors between them due to different dimensions and units, so as to better calculate the weights. The average value and standard deviation of each normalized agronomic parameter data were calculated, the coefficient of variation of each parameter was calculated through the obtained average value and standard deviation (Equation (6)), and then the weight of an index in this period was determined according to the coefficient of variation

(Equation (7)). The weighting of various indicators was carried out through the obtained weights, and the comprehensive growth index CGI<sub>cv</sub> was obtained (Table 4).

$$V_i = \frac{S_i}{\bar{X}_i} \quad (6)$$

$$\omega_i = \frac{V_i}{\sum_{j=1}^n V_j} \quad (7)$$

In the formula,  $i$  represents the category of agronomic parameters, where  $S_i$  and  $\bar{X}_i$  are respectively the standard deviation and average value of each agronomic parameter, represent the coefficient of variation calculated by this type of agronomic parameter, and  $\omega_i$  are the weight of each parameter.

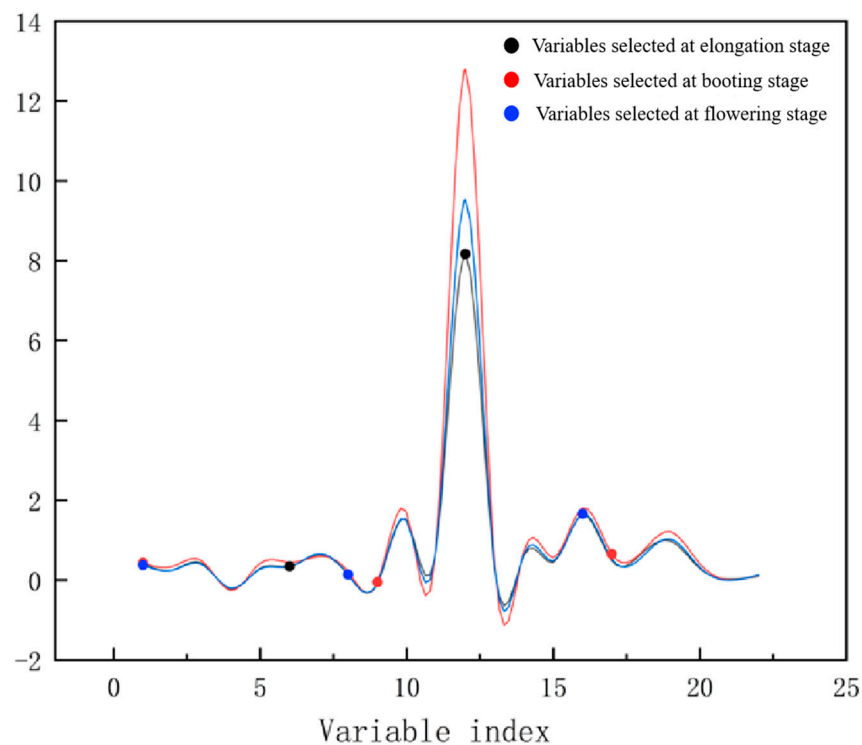


**Figure 6.** The process of filtering the characteristic parameters of each period using the SPA algorithm. Note: The black curves represent the variables selected at elongation stage, the red curve represents the variables selected booting stage, the blue curves represent the variables selected for flowering stage.

**Table 4.** The formula constructed for CGI<sub>cv</sub>, the comprehensive growth index, at each growth stage.

Growth Stage	Comprehensive Growth Indicator CGI <sub>cv</sub>
Jointing Stage	$CGI_{cv} = 0.28 \times I_{AGB} + 0.37 \times I_{SPAD} + 0.35 \times I_{LNC}$
Booting Stage	$CGI_{cv} = 0.31 \times I_{AGB} + 0.34 \times I_{SPAD} + 0.35 \times I_{LNC}$
Flowering Stage	$CGI_{cv} = 0.29 \times I_{AGB} + 0.33 \times I_{SPAD} + 0.38 \times I_{LNC}$

In order to ensure the accuracy and representativeness of the CGI constructed based on the coefficient of variation method in growth monitoring, it is necessary to further analyze the correlation between the CGI constructed based on this method and various agronomic parameters. The results are shown in Table 5. The results show that the CGI<sub>cv</sub> constructed based on the coefficient of variation method showed a very significant correlation level with the aboveground biomass, chlorophyll content, and leaf nitrogen content, indicating that CGI<sub>cv</sub> can characterize the information of various agronomic parameters of winter wheat.

**Table 5.** Correlation analysis of agronomic parameters and comprehensive index CGIcv at each growth stage.

Growth Stage	AGB	SPAD	LNCR
Jointing Stage	0.897 **	0.802 **	0.719 **
Booting Stage	0.891 **	0.816 **	0.807 **
Flowering Stage	0.862 **	0.844 **	0.799 **

Note: \*\* indicates significance at 0.01 level, respectively.

In this study, a total of 22 feature parameters was extracted using the image data captured with the drone RGB and hyperspectral cameras, and the correlation analysis was carried out with CGIcv in three periods. The results are shown in Figures 6–8. Except for VARI, NPCI, VOGI, GNDVI, MSR, TCARI and other feature parameters, the correlation levels were different in different periods, and the other feature parameters reached a very significant correlation level.

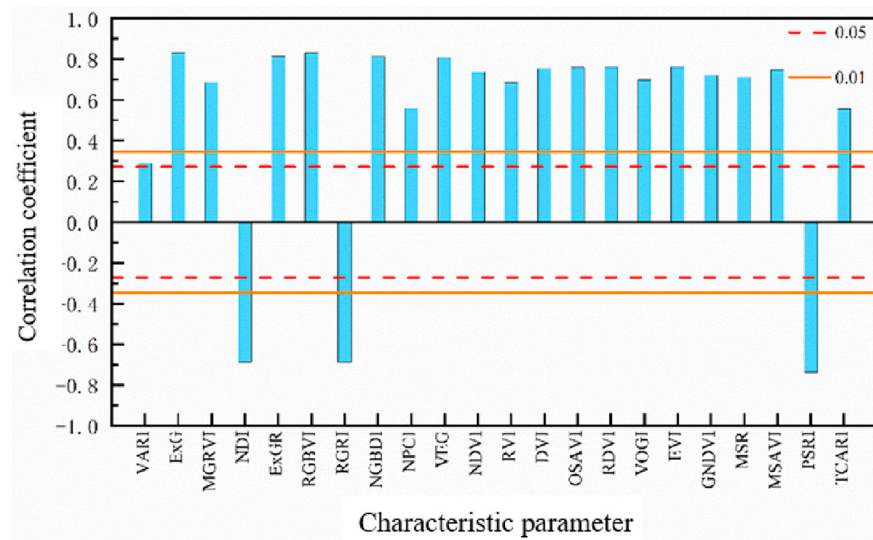


**Figure 7.** Correlation analysis between characteristic parameters at the jointing stage and comprehensive index CGIcv.

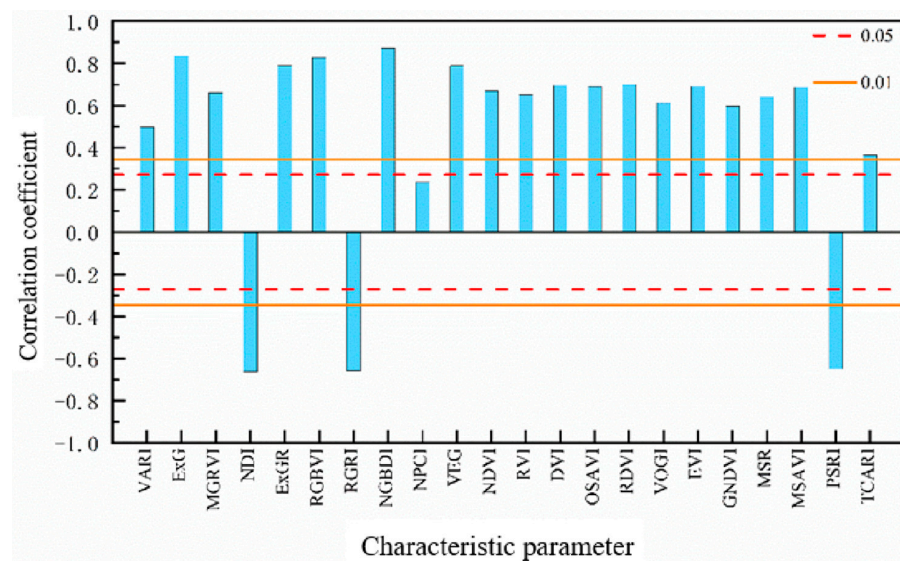


**Figure 8.** Correlation analysis between characteristic parameters t the booting stage and comprehensive index CGIcv.

Through the correlation analysis between CGIcv and each characteristic parameter in the above figure, it is concluded that there are many features that reach a very significant correlation level with the comprehensive growth index (CGI) in each period. In order to screen out better variables, the SPA algorithm was used for feature screening of 22 characteristic parameters. Figure 9 shows the variable-screening process at the jointing stage, booting stage, and flowering stage. As shown in Figure 9, the variables screened at the jointing stage are ExG, RGBVI, VEG, and OSAVI; the variables screened at the booting stage are NGBDI and GNDVI; the variables screened at the flowering stage are NPCI, VEG, and VOGI.

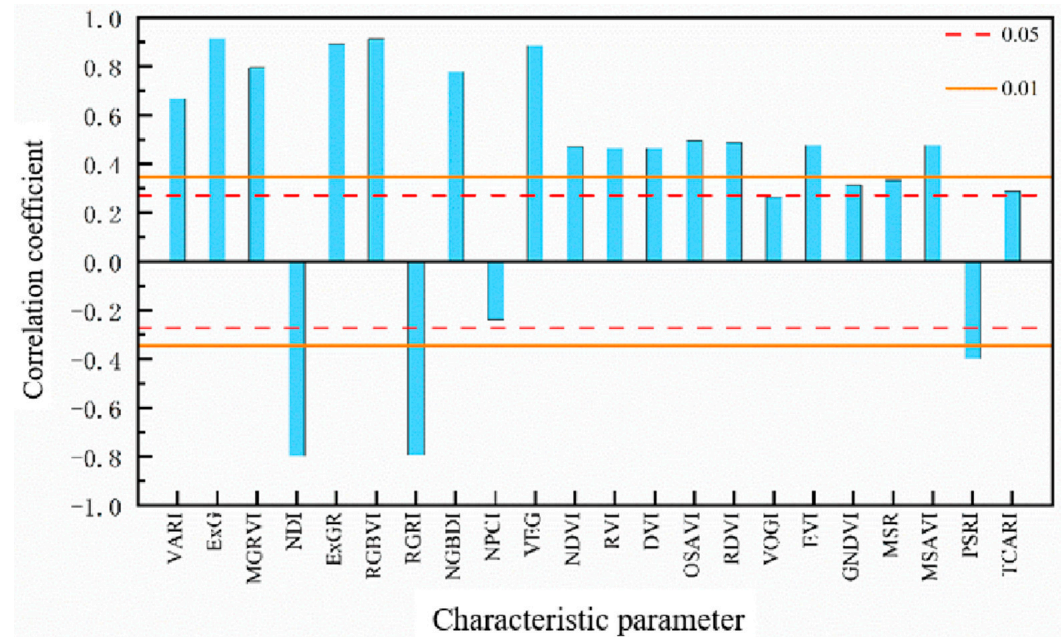


**Figure 9.** Correlation analysis between characteristic parameters at the flowering period and comprehensive index CGIcv.

### 3.2. Estimation of Comprehensive Growth Indicators Based on Drone Image Data

In this study, two new comprehensive growth indicators, CGIavg and CGIcv, were constructed by synthesizing the agronomic parameters of wheat at each growth stage, and different methods were used to construct two new comprehensive growth indicators. The correlation between the constructed indicators and the measured values reached a very significant correlation, indicating that the comprehensive growth index (CGI) can effectively reflect the growth of wheat. In addition, this study also analyzed the correlation between the characteristic parameters extracted from drone images and the comprehensive growth index (CGI) and used the SPA algorithm to screen variables to select the best variables for the construction of the comprehensive growth index (CGI) estimation model to improve the estimation accuracy.

#### 3.2.1. Model Construction and Verification of CGIavg

##### Model Building for CGIavg

According to the SPA algorithm, the characteristic parameters for the three periods were screened, the characteristic parameters screened with the SPA algorithm were used as independent variables, and the comprehensive growth potential index constructed with the equal weight method was used as the dependent variable. The CGIavg estimation model was constructed using the MSR, Gaussian process regression, and SVR methods. Table 6 shows the accuracy comparison of the MSR, GPR, and SVR models.

**Table 6.** CGIavg estimation model at each growth stage.

Growth Stage	Model	Modeling Set			Validation Set		
		R <sup>2</sup>	RMSE	NRMSE (%)	R <sup>2</sup>	RMSE	NRMSE
Jointing Stage	MSR	0.83	0.087	11.45	0.77	0.095	14.16
	GPR	0.76	0.098	12.91	0.69	0.105	15.56
	SVR	0.68	0.107	14.09	0.71	0.102	15.21
Booting Stage	MSR	0.69	0.103	13.56	0.62	0.113	13.94
	GPR	0.78	0.092	12.11	0.71	0.098	12.23
	SVR	0.73	0.096	12.64	0.67	0.106	13.08
Flowering Stage	MSR	0.76	0.095	11.59	0.69	0.104	12.93
	GPR	0.72	0.101	12.32	0.67	0.107	13.31
	SVR	0.81	0.082	10.02	0.78	0.087	10.81

It can be seen from Table 6 that the modeling set has a maximum determination coefficient R<sup>2</sup> for the MSR model at the jointing period of 0.83, which is 0.07 and 0.15 higher than that of the GPR and SVR models, respectively; the RMSE and NRMSE of the MSR model are also the smallest among the three, indicating that the accuracy of the MSR model in the modeling set is the best. At the booting stage, the determination coefficient of the GPR model was 0.78, the RMSE and NRMSE were 0.092 and 12.11%, respectively, R<sup>2</sup> was the highest among the three, and the RMSE and NRMSE were the lowest, indicating that the accuracy of the GPR model was the highest at the booting stage. Among them, the SVR model was second: its R<sup>2</sup> was 0.05 lower than that of the GPR model, and its RMSE and NRMSE were also higher than those of the GPR model; the MSR model was the worst compared with the former two. During the flowering period, the modeling R<sup>2</sup> of the three reached more than 0.7, of which the SVR model was up to 0.81; compared with the MSR model and the GPR model, the SVR showed better performance of the model with its smaller RMSE and NRMSE. Therefore, the model with the best modeling set during the flowering period is the SVR model, followed by the MSR model, and the worst model is the GPR model.

#### Model Validation of CGIavg

According to the validation dataset at the jointing stage, it is concluded that the MSR model has the highest modeling accuracy; its determination coefficient R<sup>2</sup> is the highest, and RMSE and NRMSE are the lowest. Comparing the modeling data at the growth stage with the verification data, the multivariate stepwise model is modeled. The minimum difference in the validation coefficient is 0.06, and the variation range of RMSE and NRMSE is lower than that of the GPR model; the determination coefficient of the validation set of the SVR model is higher than that of the modeling set, indicating that the model has certain overfitting. To sum up, it is concluded that the comprehensive growth index model constructed using the MSR method during the jointing period has better fitting. At the booting stage, comparing the data of the modeling set and the validation set, the validation decision coefficients of the three models are all lower than the modeling decision coefficients, and the RMSE and NRMSE increased, indicating that the three models had better fit. Compared with MSR and SVR, the GPR model has the highest determination coefficient in the data of the modeling set and validation set, and the values and variation range of RMSE and NRMSE are the smallest, indicating that at the booting stage, the comprehensive growth index model constructed by the SVR method has better predictive ability and the highest accuracy. Comparing and analyzing the data at the flowering period, the determination coefficient of the SVR model verification was significantly higher than that of the GPR and MSR models, and its RMSE and NRMSE were the smallest; the determination coefficient of SVR modeling was also the highest, and its RMSE and NRMSE variation range was also the smallest, indicating that during the flowering period, the model constructed using the SVR method had the highest accuracy. Figures 10–12 are 1:1 line graphs of the measured and predicted values of the best model for each growth period.

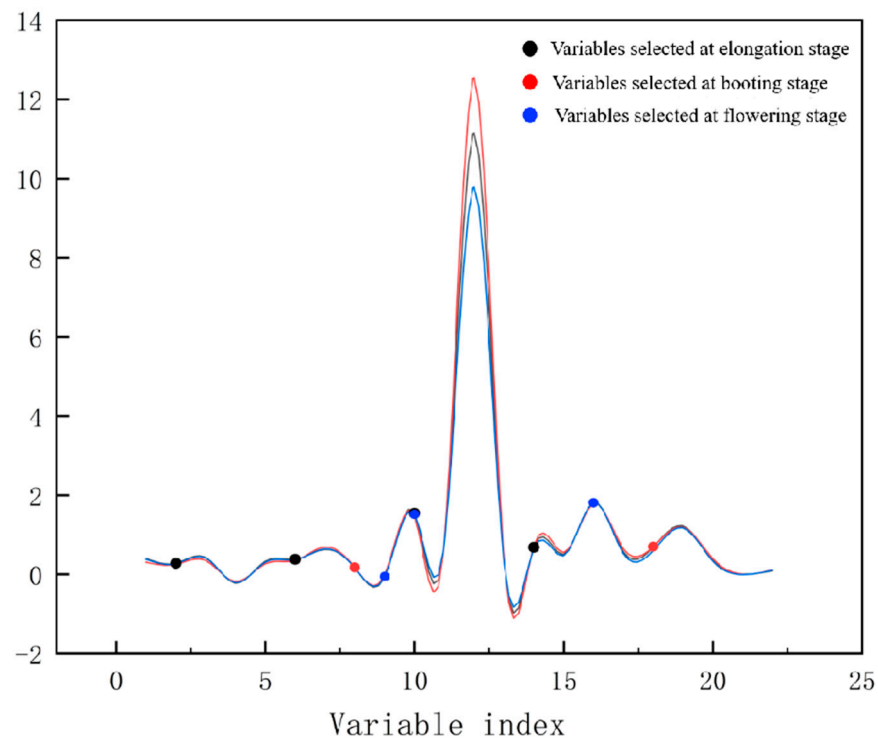


**Figure 10.** The process of filtering the characteristic parameters of each period using the SPA algorithm. Note: The black curves represent the variables selected at elongation stage, the red curve represents the variables selected booting stage, the blue curves represent the variables selected for flowering stage.

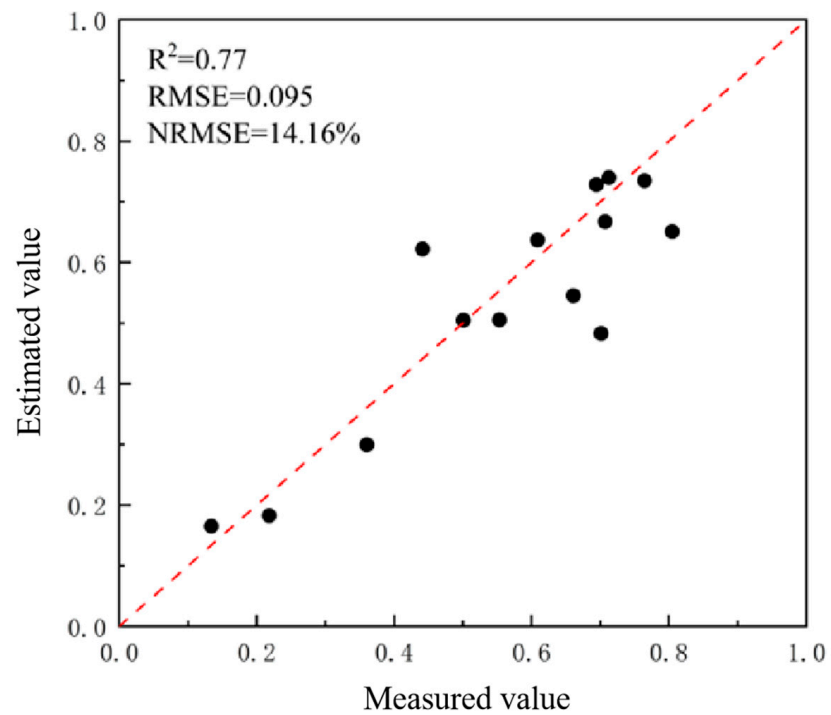


**Figure 11.** Scatterplot with a 1:1 reference line of CGIavg measured and predicted values for the SVR model validation set at the jointing stage.

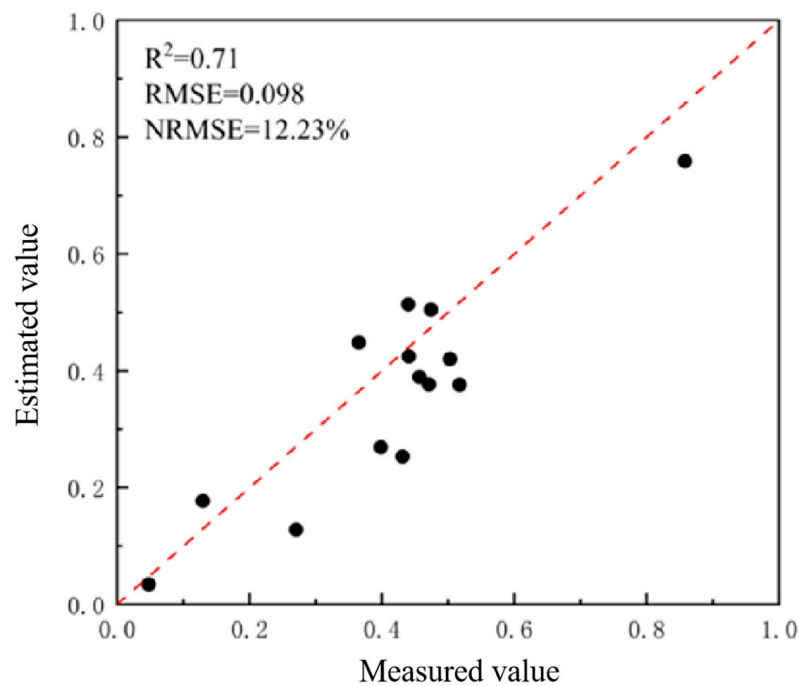


**Figure 12.** Scatterplot with a 1:1 reference line of CGIavg measured and predicted values in the booting stage GPR model validation set.

### 3.2.2. Model Construction and Verification of CGICV

#### Model Construction of CGICV

According to the SPA algorithm, the characteristic parameters of the three periods were screened, the characteristic parameters screened with the SPA algorithm were used as independent variables, and the comprehensive growth index (CGI) constructed using the coefficient of variation method was used as the dependent variable. MSR, GPR, and SVR were used to construct the CGIcv estimation model. Table 7 shows the accuracy comparison of the MSR, GPR, and SVR models.

**Table 7.** CGIcv estimation model for each growth stage.

Growth Stage	Model	Modeling Set			Validation Set		
		$R^2$	RMSE	NRMSE	$R^2$	RMSE	NRMSE
Jointing Stage	MSR	0.77	0.075	10.12	0.73	0.084	14.21
	GPR	0.71	0.087	11.85	0.74	0.079	13.67
	SVR	0.66	0.094	12.74	0.63	0.098	16.96
Booting Stage	MSR	0.65	0.107	14.05	0.51	0.128	15.77
	GPR	0.80	0.087	11.42	0.74	0.092	12.31
	SVR	0.78	0.090	11.85	0.72	0.096	12.61
Flowering Stage	MSR	0.75	0.087	12.08	0.69	0.102	14.16
	GPR	0.71	0.092	12.78	0.66	0.113	15.69
	SVR	0.84	0.077	10.69	0.78	0.085	11.82

It can be seen from Tables 4 and 5 that the determination coefficient  $R^2$  of the GPR and MSR models of the modeling set at the jointing stage is above 0.7, among which the determination coefficient of the MSR model is above 0.75, while the determination coefficient of the SVR at the jointing stage is only 0.66. Comparing the RMSE and NRMSE of the three, it is found that the MSR model is the lowest, indicating that the modeling effect during the jointing stage is the best in the MSR model, the GPR model is second, and the SVR model is the worst. At the booting stage, the determination coefficient of the GPR model is the highest at 0.8, the SVR is slightly lower at 0.02, and the MSR model is the

smallest; among them, the RMSE and NRMSE are also the smallest for GPR, indicating that the GPR model has the best modeling accuracy at the booting stage. During the flowering period, the determination coefficient, RMSE, and NRMSE of the SVR model were 0.84, 0.077, and 10.69%, respectively. The determination coefficients were the highest among the three, and the remaining two indicators were the lowest among the three, indicating that the model with the best modeling effect during the flowering period was the SVR model, after which the MSR model was the second, and the GPR model was the worst.

#### Model Validation of CGICV

According to the data verification at the jointing stage, the determination coefficient of the GPR model and the MSR model is above 0.7, while the SVR model is significantly lower; comparing the data of the modeling set and the validation set, it is found that the verification determination coefficient of the GPR model at the jointing stage is higher than that of the modeling. The determination coefficient of the model shows a certain overfitting phenomenon; while the RMSE and NRMSE of the MSR model are the lowest, combined with the above analysis, the best modeling method in the jointing stage is the MSR model. In the validated  $R^2$  at the booting stage, the GPR and SVR models were above 0.7, while the  $R^2$  of the MSR model was only 0.51; comparing the changes in RMSE and NRMSE before and after the GPR and SVR models, it was found that the variation range of the GPR model was small, indicating that the GPR model was the best modeling method at the booting stage. At the flowering stage, only the determination coefficient of the SVR model was above 0.7, and the verification accuracy of the remaining two models was not high; comparing the data before and after, the changes in the RMSE and NRMSE before and after the SVR model were the smallest, followed by the MSR, and the accuracy of the GPR model was the worst. In summary, the optimal model at the flowering stage was the SVR model. Figures 13–16 are 1:1 line graphs of the best model measured and predicted values for each growth period.

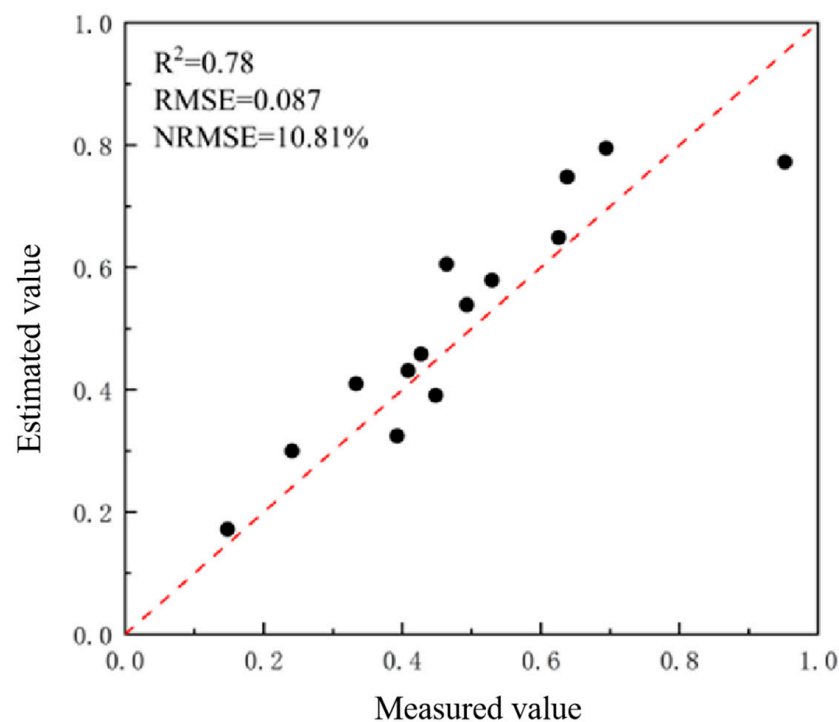


**Figure 13.** Scatterplot with a 1:1 reference line of CGIavg measured and predicted values for the SVR model validation set at the flowering stage.

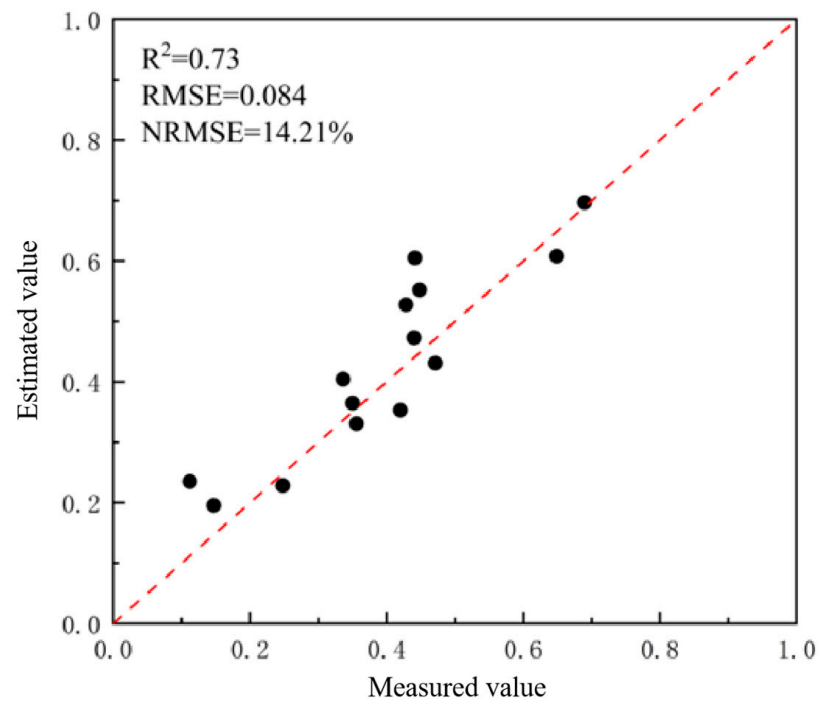


**Figure 14.** Scatterplot with a 1:1 reference line of the measured and predicted values of the MSR model validation set CGIcv at the jointing stage.

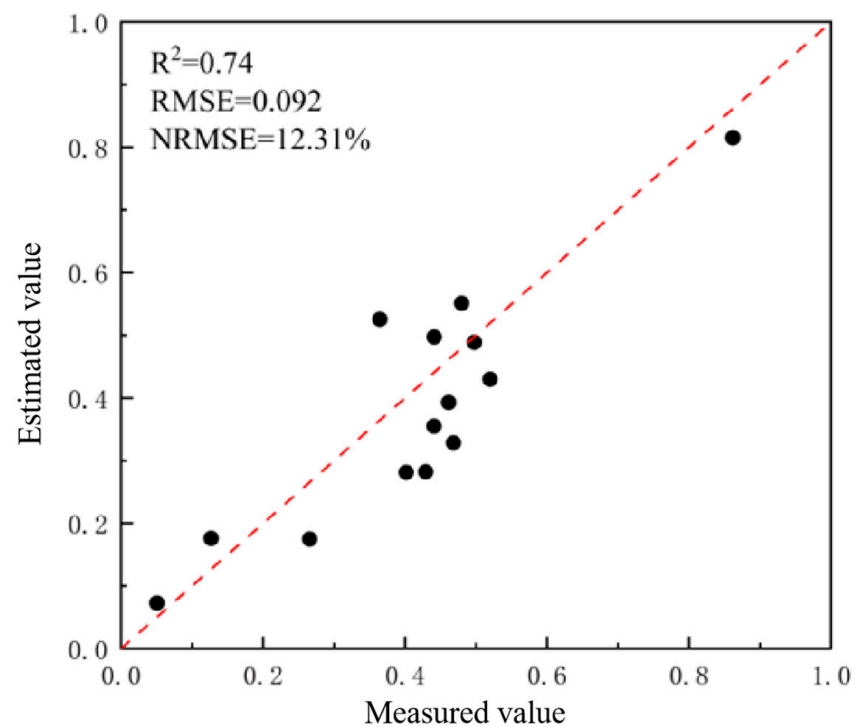


**Figure 15.** Scatterplot with a 1:1 reference line graph of the measured and predicted values of the GPR model validation set CGIcv at the booting stage.

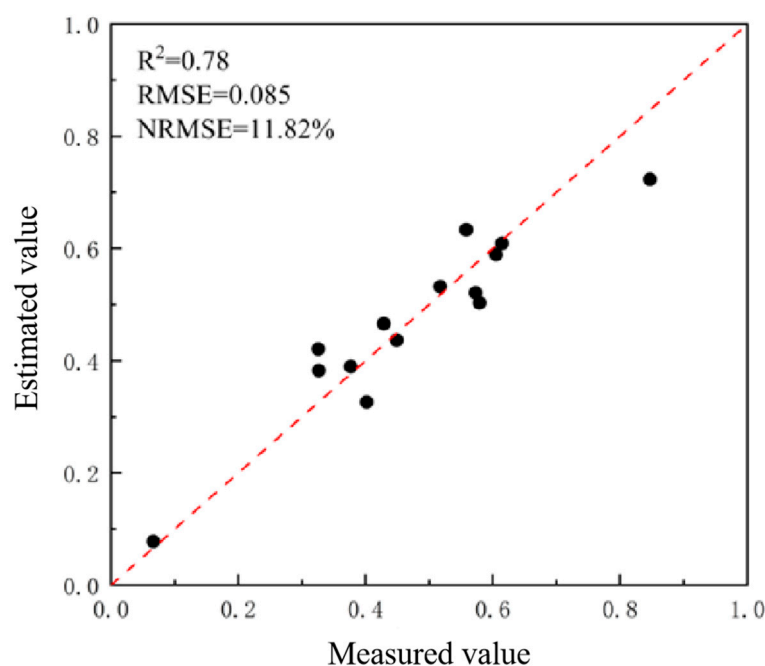


**Figure 16.** Scatterplot with a 1:1 reference line of the measured and predicted values of the SVR model validation set CGIcv at the flowering stage.

#### 4. Discussion

In the growth monitoring of crops, the growth status of crops can be analyzed by obtaining various agronomic parameters of the crops, laying a foundation for guiding agricultural production and ensuring sustainable agricultural development [22]. With the rise of drone remote sensing technology, more and more researchers use drone platforms to remotely monitor crop growth indicators. Based on drone remote sensing data, this study estimates agronomic parameters and comprehensive growth indicators for the three key growth stages of wheat. Hasan et al. [23] used the characteristic parameters extracted from drone RGB images to estimate the leaf area index of winter wheat. Compared with this study, although the parameters of hyperspectral images are missing on the drone sensor, the optimal parameters selected by gray correlation analysis are used. The combination of parameters constructs a high-precision estimation model of the leaf area index, indicating that the diversification of the input sources of modeling parameters may not necessarily optimize the estimation model. Effective screening of variables is very meaningful for the construction of the later model. Shu et al. [24], when remote sensing monitoring the biomass of maize, added plant height and texture characteristics to effectively improve the estimation accuracy. When estimating a single agronomic index, this study only considered the category of drone images, and did not introduce other types of data for auxiliary modeling to find the optimal estimation model.

There are also certain differences between different data sources to construct comprehensive indicators. Zhai et al. [6] constructed comprehensive growth indicators based on the nitrogen content, chlorophyll content, and plant water content of winter wheat canopy leaves. Although there is only one difference in the agronomic indicators, the inversion accuracy of comprehensive indicators is obviously better than that of a single indicator. Wang et al. [8] used six winter wheat growth indicators including the leaf area index, above-ground dry biomass, above-ground fresh biomass, plant water content, chlorophyll density, and nitrogen accumulation, as well as winter wheat canopy hyper spectroscopy. Principal component analysis was introduced to construct a comprehensive growth index (CGI) that could characterize the growth of winter wheat, and it was combined with the partial least squares regression method to construct a hyperspectral estimation model of the CGI. Compared with this study, in the case of multiple agronomic parameters, the accuracy of the CGI hyperspectral monitoring model is better. In growth monitoring, the method of

constructing comprehensive growth indicators is better than that of a single parameter to a certain extent. When using drone images to monitor crop growth, multiple data are of course important, but under limited conditions, using new index synthesis to evaluate crop growth is also a new research approach. Compared with other researchers' studies, our CGI can obtain more accurate data in a smaller measurement size and scope and has provided a more reasonable assessment of the growth of winter wheat. At the same time, compared with the current methods of evaluating winter wheat growth, CGI can greatly improve the evaluation efficiency, save time and labor costs, and be applied to more farming scenarios. Finally, this study is limited to a single winter wheat crop, and this paper only studies the comprehensive growth monitoring of winter wheat, without considering the monitoring and estimation of other crops. Therefore, the study can be extended to other crops in the future, so as to obtain a more extensive application value.

## 5. Conclusions

The equal weight method and the coefficient of variation method were introduced to construct the comprehensive growth indicators CGI<sub>avg</sub> and CGI<sub>cv</sub>. From previous studies, it has been shown that the growth change status reflected by a single crop growth index is very limited to a certain extent, so the comprehensive growth index (CGI) is introduced to more comprehensively and reasonably characterize the growth and development status of crops. In this study, three agronomic parameters of aboveground biomass, leaf nitrogen content, and chlorophyll content were selected when constructing the comprehensive growth index (CGI). The aboveground biomass reflects the total amount of organic matter contained in wheat plants. Changes in chlorophyll content can reflect the photosynthetic efficiency and growth status of wheat. Changes in the leaf nitrogen content can reflect the efficiency and quantity of wheat protein synthesis. Based on the fact that all three are the dominant factors affecting wheat growth, two different methods were used to construct comprehensive growth indicators to characterize the growth status of wheat. Comparing the estimation models using a single index and comprehensive growth index (CGI) in each period, it is found that the estimation model of the comprehensive growth index (CGI) has higher accuracy.

Nowadays, we are moving towards the era of precision agriculture. The technology of monitoring wheat growth with drones has been used in various fields. Monitoring wheat growth using a comprehensive growth index is of significance to agricultural administrators. In the future, more monitoring indicators can be introduced into the model to improve the spatial and temporal resolution of the data, and we can adopt more advanced remote sensing technology and data processing methods to improve the accuracy and reliability of wheat comprehensive growth monitoring.

**Author Contributions:** Conceptualization, Y.T.; methodology, Y.Z.; software, M.C.; validation, C.S.; formal analysis, M.C.; investigation, Y.T.; resources, Y.Z.; data curation, Y.T.; writing—original draft preparation, Y.T.; writing—review and editing, C.S.; visualization, Y.Z.; supervision, C.S.; project administration, C.S.; funding acquisition, M.C. All authors have read and agreed to the published version of the manuscript.

**Funding:** Key Research and Development Program (Modern Agriculture) of Jiangsu Province (BE2022335, BE2022338); National Natural Science Foundation of China (31872852); National Key Research and Development Program of China (2018YFD0300805).

**Data Availability Statement:** The data provided in the article are all available.

**Acknowledgments:** Thanks to the project funded by the Priority Academic Program Development of Jiangsu Higher Education Institutions (PAPD), and to Yangzhou University for providing the scientific research platform.

**Conflicts of Interest:** The authors declare no conflict of interest.

## References

1. Chen, K.; Tian, G.; Tian, Z.; Ren, Y.; Liang, W. Evaluation of the Coupled and Coordinated Relationship between Agricultural Modernization and Regional Economic Development under the Rural Revitalization Strategy. *Agronomy* **2022**, *12*, 990. [[CrossRef](#)]
2. Khan, N.; Ray, R.L.; Kassem, H.S.; Zhang, S. Mobile Internet Technology Adoption for Sustainable Agriculture: Evidence from Wheat Farmers. *Appl. Sci.* **2022**, *12*, 4902. [[CrossRef](#)]
3. Feng, H.; Tao, H.; Li, Z.; Yang, G.; Zhao, C. Comparison of UAV RGB Imagery and Hyperspectral Remote-Sensing Data for Monitoring Winter Wheat Growth. *Remote Sens.* **2022**, *14*, 3811. [[CrossRef](#)]
4. Zhao, X.; Na, X. Study on Remote Sensing Monitoring of Crop Growth Based on Comprehensive Index: A Case Study of the Songnen Plain. *Geogr. Geo-Inf. Sci.* **2022**, *33*, 12–18.
5. Zhou, S.; Huang, Z. Remote sensing monitoring of winter wheat growth in Hebei province based on comprehensive indicators. *J. Hengyang Norm. Univ.* **2021**, *42*, 82–87.
6. Liu, F.; Liu, Y.; Su, L.; Tao, W.; Wang, Q.; Deng, M. Integrated Growth Model of Typical Crops in China with Regional Parameters. *Water* **2022**, *14*, 1139. [[CrossRef](#)]
7. Ji, H.; He, X.; Wang, W.; Zhang, H. Prediction of Winter Wheat Harvest Based on Back Propagation Neural Network Algorithm and Multiple Remote Sensing Indices. *Processes* **2023**, *11*, 293. [[CrossRef](#)]
8. Wang, C.; Wang, J.; Feng, M.; Xiao, L.; Sun, H.; Xie, Y.; Yang, W. Hyperspectral estimation on growth status of winter wheat by using the multivariate statistical analysis. *Spectrosc. Spectr. Anal.* **2018**, *38*, 1520–1525.
9. Gao, L.; Yang, G.; Li, H.; Feng, H.; Wang, L.; Dong, J.; He, P. Leaf area index detection of winter wheat based on drone digital image. *Chin. J. Eco-Agric.* **2016**, *24*, 1254–1264.
10. Cao, Z.; Li, Y.; Huang, J.; Ye, C.; Sun, B.; Shu, S.; Zhu, Y.; He, Y. Monitoring Rice Leaf Area Index Based on Unmanned Aerial Vehicle (UAV) Digital Images. *Chin. J. Rice Sci.* **2022**, *36*, 308–317.
11. Song, Y.; Chen, Y.; Yang, J.; Liu, T.; Li, D.; Sun, C. Identification of wheat scab by digital image color feature index. *Jiangsu Agric. Sci.* **2022**, *50*, 186–191.
12. Teng, J.; Liu, Y.; Ding, M. The Evaluation of Efficiency of Color Metrics in Monitoring *Robinia Pseudoacacia* Phenology based on RGB Images. *Remote Sens. Technol. Appl.* **2018**, *33*, 476–485.
13. Liu, H.; Bruning, B.; Garnett, T.; Berger, B. The Performances of Hyperspectral Sensors for Proximal Sensing of Nitrogen Levels in Wheat. *Sensors* **2020**, *20*, 4550. [[CrossRef](#)] [[PubMed](#)]
14. Liu, L.; Dong, Y.; Huang, W.; Du, X.; Ma, H. Monitoring Wheat Fusarium Head Blight Using Unmanned Aerial Vehicle Hyperspectral Imagery. *Remote Sens.* **2020**, *12*, 3811. [[CrossRef](#)]
15. Hu, J.; Peng, J.; Zhou, Y.; Xu, D.; Zhao, R.; Jiang, Q.; Fu, T.; Wang, F.; Shi, Z. Quantitative Estimation of Soil Salinity Using UAV-Borne Hyperspectral and Satellite Multispectral Images. *Remote Sens.* **2019**, *11*, 736. [[CrossRef](#)]
16. Fu, Z.; Jiang, J.; Gao, Y.; Krienke, B.; Wang, M.; Zhong, K.; Cao, Q.; Tian, Y.; Zhu, Y.; Cao, W.; et al. Wheat Growth Monitoring and Yield Estimation based on Multi-Rotor Unmanned Aerial Vehicle. *Remote Sens.* **2020**, *12*, 508. [[CrossRef](#)]
17. Wu, J.; Shen, S.; Dong, J.; Li, H.; Chen, Y.; Mao, W. Crop nitrogen content detection method by AOTF hyper-spectral imaging. *Sens. Microsyst.* **2017**, *36*, 64–67.
18. Cheng, Z.; Zhang, L.; Liu, H.; Zhu, A. Continuous projection algorithm and its application in wavelength selection of near-infrared spectroscopy of wheat. *Spectrosc. Spectr. Anal.* **2010**, *30*, 949–952.
19. Yang, B.; Chen, S.; Yu, H.; An, Q. Remote sensing estimation of rice yield based on random forest regression method. *J. China Agric. Univ.* **2020**, *25*, 26–34.
20. Liang, L.; Yang, M.; Zang, Z. Hyperspectral determination of nitrogen content in wheat canopy based on wavelet denoising and SVR. *Trans. Chin. Soc. Agric. Eng.* **2010**, *26*, 248–253.
21. Jing, X.; Zhang, T.; Zou, Q.; Yan, L.; Dong, Y. Remote sensing monitoring model of wheat stripe rust based on fractional differential spectral index. *Trans. Chin. Soc. Agric. Eng.* **2021**, *37*, 142–151.
22. Zhuo, Y.; Ding, F.; Yan, H.; Xu, J. Advances in forage crop growth monitoring by UAV remote sensing. *Smart Agric.* **2022**, *4*, 35–48.
23. Hasan, U.; Sawut, M.; Chen, S. Estimating the leaf area index of winter wheat based on unmanned aerial vehicle RGB-image parameters. *Sustainability* **2019**, *11*, 6829. [[CrossRef](#)]
24. Shu, M.; Shen, M.; Dong, Q.; Yang, X.; Li, B.; Ma, Y. Estimating the maize above-ground biomass by constructing the tridimensional concept model based on UAV-based digital and multi-spectral images. *Field Crops Res.* **2022**, *282*, 108491.

**Disclaimer/Publisher's Note:** The statements, opinions and data contained in all publications are solely those of the individual author(s) and contributor(s) and not of MDPI and/or the editor(s). MDPI and/or the editor(s) disclaim responsibility for any injury to people or property resulting from any ideas, methods, instructions or products referred to in the content.